Eurographics Symposium on Rendering (2022)
A. Ghosh and L.-Y. Wei (Editors)

Planetary Shadow-Aware Distance Sampling

Carl Breyer[1] and Tobias Zirr[1]

[1]Karlsruhe Institute of Technology

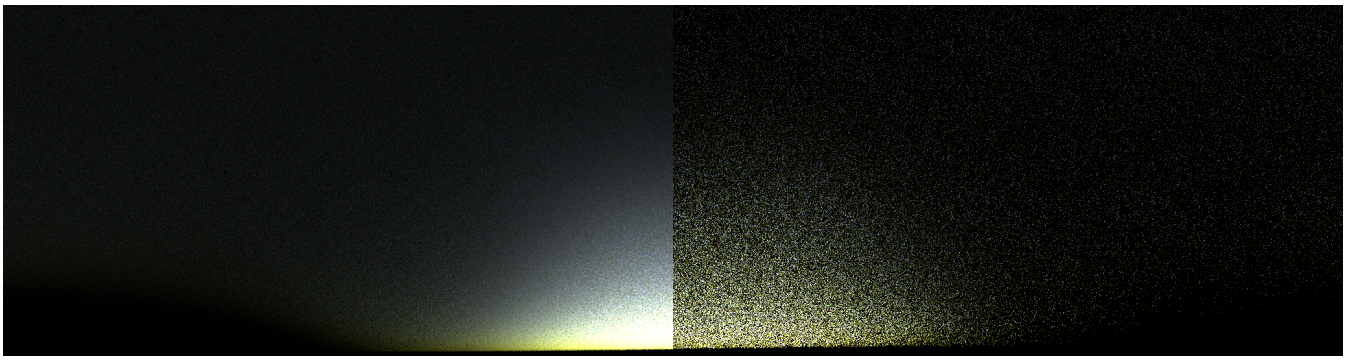

Figure 1: *Path-traced single scattering at 32 samples per pixel, rendered with (left) and without (right) our shadow-aware distance sampling in the atmospheric volume, for a simple model (see Sect. 4) with spectral Rayleigh and Mie scattering. The star is 5.711° below the horizon.*

Abstract

Dusk and dawn scenes have been difficult for brute force path tracers to handle. We identify that a major source of the inefficiency in explicitly path tracing the atmosphere in such conditions stems from wasting samples on the denser lower parts of atmosphere that get shadowed by the planet before the upper, thinner parts when the star sets below the horizon. We present a technique that overcomes this issue by sampling the star only from the unshadowed segments along rays based on boundaries found by intersecting a cylinder fit to the planet's shadow. We also sample the transmittance by mapping the distances of the boundaries to opacities and sampling the visible segments uniformly in opacity space. Our technique can achieve similar quality compared to brute-force path tracing at around a 60th of the time in such conditions.

CCS Concepts

• ***Computing methodologies*** → ***Ray tracing; Visibility;***

1. Introduction

Having a good representation of the atmosphere is an important part of rendering outdoor scenes. Conventionally, this has been achieved via analytical sky models [PSM93, PSS99, HW12]. This comes with the drawback that things like areal perspectives are neglected. Such effects can be naturally included in a brute force Monte Carlo simulation of the atmosphere. The issue is that a straightforward implementation of such path tracing is rather inefficient and impractical for production purposes.

A configuration where brute force path tracers perform poorly is when the star is below the horizon. We found that this is primarily due to most distances sampled in the atmospheric volume ending up within the planet's shadow. The distance samples that make it out of the shadow are rare, thus many samples per pixel are required for the thinner upper unshadowed parts to be sufficiently sampled. See Fig. 2 for an illustration.

We write the generic integral of radiance from all shadowed and unshadowed connections between an atmospheric medium and a radiant star illuminating a planet, scattered at any distance t, as:

$$L_o(\mathbf{x},\omega_o) = \int_0^\infty T(t)\,\mu_s(t)\left(\int_\Omega P(\omega_o,\omega)\,L_i(t,\omega)V_i(t,\omega)\,\mathrm{d}\omega\right)\mathrm{d}t, \quad (1)$$

where

- μ_s and μ_t are the scattering and extinction coefficients,
- $T(t) := e^{-\int_0^t \mu_t(s)ds}$ is the transmittance,
- $P(\omega_o,\omega)$ is the phase function,
- $L_i(t,\omega)$ is the incoming radiance from the light source, and
- $V_i(t,\omega)$ is the incoming visibility, 0 in shadows and 1 otherwise.

DOI: 10.2312/sr.20221152

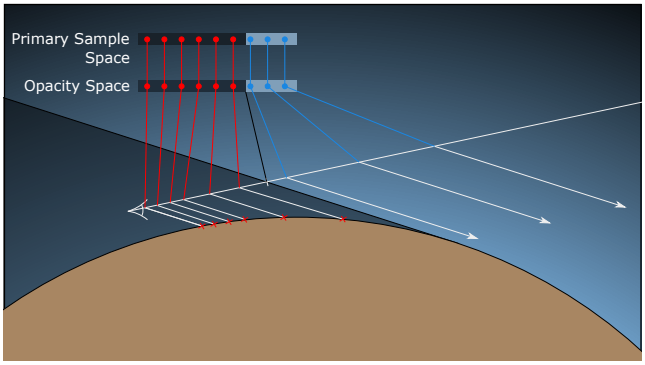

Figure 2: *Along a camera ray, the density of connections between an atmospheric volume and an illuminating star is high near the ground level, even when the sampled segments are largely in the planetary shadow due to the star being below the horizon.*

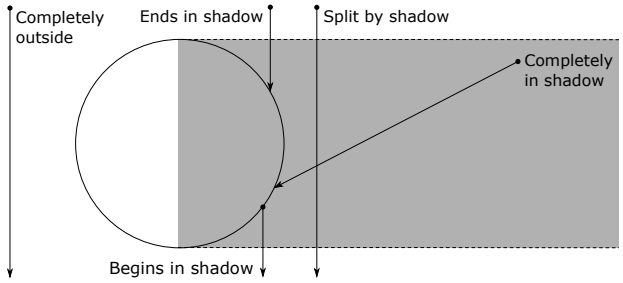

Figure 3: *When identifying unshadowed segments for shadow-aware distance sampling along one ray with one shadow cylinder, there are five cases resulting in 0, 1, and 2 unshadowed segments.*

Since shadowed connections contribute zero radiance, we can restrict the integration domain to the parts where the incoming visibility is non-zero. Our novel contribution is a specialization of this approach to the shadow of a planet that is illuminated by a reasonably distant star, which results in tractable analytical computations of integral boundaries: We swap the order of integration for light directions and free paths, and we fit an analytical cylinder to the planetary shadow resulting for each light direction. We seek the distances a_i, b_i where an unshadowed segment begins and ends:

$$L_o(\mathbf{x},\omega_o) = \int_\Omega \sum_{j=1}^{n(\mathrm{x},\omega)} \int_{a_j}^{b_j} T(t)\,\mu_s(t) P(\omega_o,\omega)\,L_i(t,\omega) V_i(t,\omega)\,\mathrm{d}t\,\mathrm{d}\omega, \quad (2)$$

where $n(\mathrm{x},\omega)$ is the number of unshadowed segments. Since we deal with just one occluding sphere in this work, the above can be specialized to five cases with a maximum of two unshadowed ray segments, as illustrated in Fig. 3. Note that in the unshadowed segments, the visibility term still needs to be included because of occlusion from terrain features like hills and mountains that deviate from the ideal sphere assumed by the cylinder fit.

2. Prior Work

In the following, we briefly discuss the related prior work on rendering of volumetric effects, rendering the atmosphere, and visibility-aware importance sampling techniques.

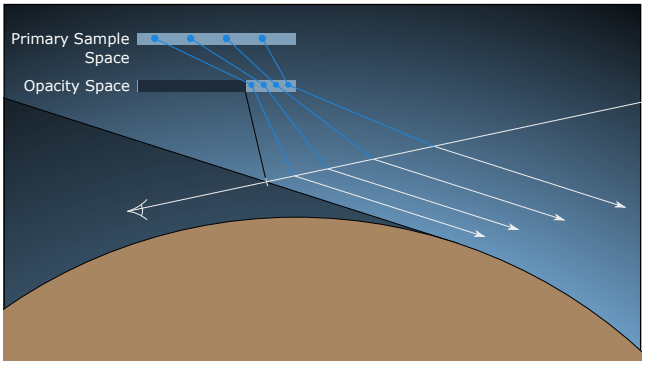

Figure 4: *Shadow-aware distance sampling re-assigns the sample mass of distances within denser, shadowed segments to thinner, unshadowed segments. Our technique directly maps all samples from primary sample space to distances past the shadow boundary.*

2.1. Importance Sampling for Volumetric Rendering

To improve importance sampling of emitter connections in volumetric rendering, techniques like equi-angular sampling [KF12] and joint importance sampling [GKH*13] account for the interplay of scattering and the geometry term in cases of direct single-scattering and indirect multiple-scattering connections. In contrast, our technique concerns itself with transmittance and visibility terms, which proves particularly relevant for atmospheric scattering. The ideas of our technique could also be applied to the aforementioned schemes in order to also account for visibility. In terms of Georgiev et al. [GKH*13], we construct a 1-random-decision subpath for transmittance and visibility instead of addressing geometry terms.

Distance samples have been restricted to intervals of relevant contribution in various contexts, e.g. to optimize volume caustics from triangle meshes [Hol15], or to prioritize important volumes confined within certain boundaries using normalized distance sampling (NDS) [VWF18], where other contributions are negligible or trivial (e.g. background illumination). Our shadow-aware distance sampling is a specialization of NDS, where we simply cut away the opacity intervals corresponding to shadowed ray segments.

2.2. Models for Atmospheric Rendering

Detailed optical models of the sky have been built [GGJ18] that can be used as inputs to path tracing techniques like ours. Conventionally, however, skies in virtual scenes have been represented as infinitely far away light sources at ground level [PSM93, PSS99, HW12]. These models do not cover areal perspectives or high altitudes, and they typically do not handle post-sunset conditions. Preetham et al. [PSS99] propose a model for areal perspectives. Vevoda and Wilkie et al. [WVBR*21] present a sky model that overcomes the above shortcomings, at the cost of extra complexity.

Bruneton [Bru17] compares recent sky models and discusses pre-computation of sky light for pre-set configurations as a natural alternative to model fitting. Single [NSTN93] and multiple scattering [NDN96, HMS05] can be taken into account for various altitudes and settings, at the cost of additional storage or recomputation for every parameter set. Hillaire [Hil20] approximates infinite bounces via a transfer function from double scattering to higher orders.

2.3. Visibility-Aware Integration

Analytically approximating the shadow of the earth by fitting a cylinder was done previously [Irw96] to accelerate ray marching-based integration and to only integrate along visible segments with the adaptive Simpson quadrature; Nishita et al. [NSTN93] use the information to disregard scattering along the shadowed part of a ray during their numerical integration. Our application is the first to our knowledge to apply this insight to modern Monte Carlo path tracers.

Billen and Dutre [BD16] analytically compute integrals over visible line segments for simple shading models like Phong [Pho75]. Salesin and Jarosz [SJ19] lift this restriction, numerically integrating other terms with Monte Carlo integration and deriving a method of visibility-aware direction sampling. Cheng [Che21] applies the ideas to volumetric shadows, constructing a shadow triangle with a point on the light and a ray going through a medium. Our formulation is more straightforward, fitting a shape to the shadow and ray-intersecting it like a physical object. Volumetric beam estimators typically integrate on the support of kernels centered around photon points, beams or higher-order primitives [HGJ*17, BJ17].

Also in real-time volume rendering, integrating visibility along a ray through a medium has been done by decomposing it into a sum of integrals over visible segments [WR08, BSA10, BCRK*10, CBDJ11]. Velinov and Mitchell [VM22] handle visible segments using a moment approximation to the resulting integrals, for the special case of light entering through rectangular windows.

3. Algorithm

We solve Eq. (2) using a specialized Monte Carlo (MC) estimator for collisions with media that are subsequently connected to the light source via next event estimation (NEE). This specialization requires two changes to standard estimators of volume transport: Firstly, the random decision whether to use NEE on the next collision in the path tracer needs to be made before performing the sampling of its distance. This is in line with previous volume sampling optimizations tailored to NEE connections like equi-angular sampling [KF12]. Secondly, for NEE, a direction towards the star needs to be sampled, and an analytic intersection with a corresponding planetary-enclosing shadow cylinder needs to be performed in order to compute the shadow boundaries that bound intervals of unshadowed volumetric interactions. The distance sampling mass is then confined to these intervals (illustrated in Fig. 4), similarly to previous optimizations like normalized distance sampling (NDS) [VWF18] (which increases the mass in intervals of volumes that need more samples).

3.1. NEE with Shadow Boundary Computation

The planetary shadow from a point on the sun is a cone, but when such a point is far away, it is approximately a cylinder. We exploit this by importance sampling emitter directions rather than points, neglecting any parallax in our variance reduction: Thus, we can already sample emitter directions at distance 0, rather than waiting for the subsequently sampled distance. The benefit of a cylinder around a fixed direction is numerical stability, as ray intersections with such a long and thin cone proved unstable in our tests.

We begin shadow-aware distance sampling and NEE by sampling a direction from the solid angle subtended by the star. We fit a cylinder to the boundary of the planet's shadow, originating at its center. The cylinder radius conservatively follows the lowest planetary elevation depicted in the scene. Its main axis is along the sampled light direction. The shadow cylinder needs to be bounded at the shadow terminator to not extend into the fully lit side of the planet.

3.2. Construction of the Shadow-Aware Distance Sampler

Our algorithm only changes volume sampling for cases of subsequent direct connections to emitters by NEE. We start with the interval $I := [I_1, I_2]$ of distances sampled along a ray that are within the atmospheric volume, cutting off any segments where gas concentrations are negligible. We then construct up to two subintervals A and B containing all distances outside the planetary shadow, by intersecting the shadow cylinder with the current ray. Since we deal with one shadow caster, we hard-coded the following cases (see Fig. 3):

- If there are no shadow intersections, keep $A = I$ and set $B = \emptyset$.
- For two intersections at distances $d_1 < d_2$ in front of the ray origin, set $A = [I_1, d_1]$ and $B = [d_2, I_2]$.
- Otherwise, if the normal of the cylinder interaction aligns with the ray (pointing outwards), set $A = [d_1, I_2]$ and $B = \emptyset$.
- Otherwise, for rays pointing inwards, set $A = [I_1, d_1]$ and $B = \emptyset$.

To sample distances within the unshadowed intervals A and B, with densities proportional to transmittances therein, we apply inverse CDF sampling piece-wise: We invert the transmittance function on each interval and use the result to map uniform primary samples to distance samples within each interval (as illustrated for one interval in Fig. 4). In our case, we work with only numerically invertible analytic models of heterogeneous atmospheric media (see Sect. 4). With more complex heterogeneous media (e.g. grid-based models), more sophisticated tracking methods may be required for distance sampling, for which Villemin et al. [VWF18] provide the extensions that allow the focusing of samples onto distance intervals. They also observe that distance sampling is equivalent to inverting the (uniformly distributed) ray segment opacities, which provide a useful abstraction for (re-)allocating uniform samples to subintervals.

3.3. Computing the Probability Density Function (PDF)

Since we merely cut away shadowed intervals from the otherwise uniformly sampled intervals of CDF values resp. opacities (for NDS [VWF18]), the only change required to compute the distance PDF is to account for the resulting uniform compression of density in the unshadowed distance intervals A and B. The increase in density is therefore $\frac{|T(I)|}{|T(A)|+|T(B)|}$, where $T(t)$ is applied to each interval boundary. For emitter direction PDFs, note sampling at distance 0.

3.4. Numerical Considerations

To avoid catastrophic cancellation, the optical depth τ should be converted to opacity using the function $\texttt{expm1}(x) = e^x - 1$ to compute $1 - e^{-\tau}$ as $-\texttt{expm1}(-\tau)$. Such a special-purpose function is typically provided by standard math libraries (e.g. the C math library). Computing sphere and cylinder intersections at planetary scales can be numerically challenging. In order to improve precision, robust quadratic equation solvers should be used.

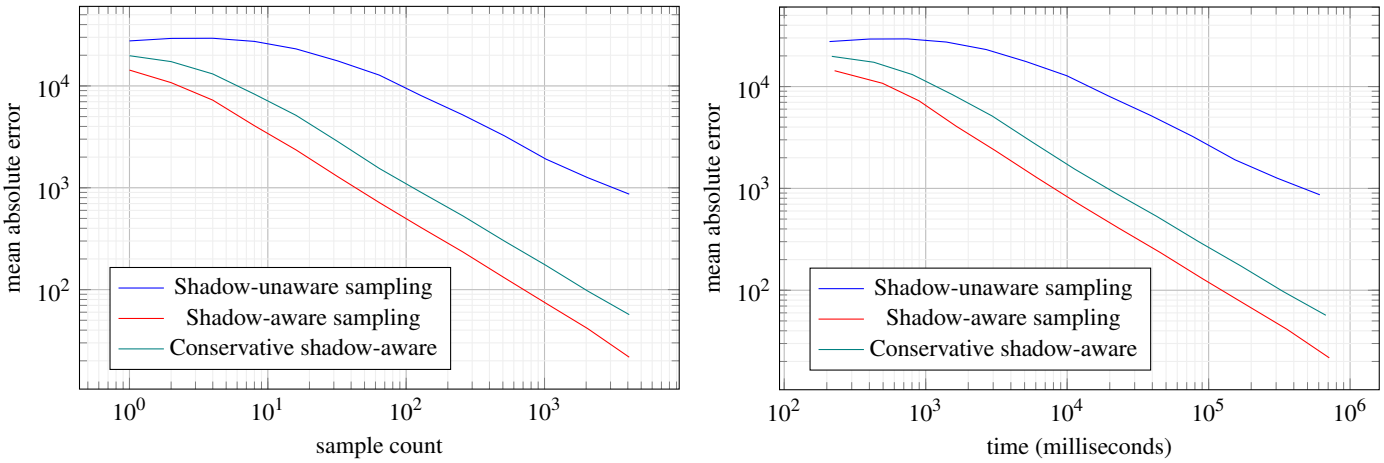

Figure 5: *Mean absolute error plotted against sample count (left) and render time (right) for shadow-aware and -unaware distance sampling. Measurements are shown for single scattering in a configuration akin to Fig. 1, with spectral Rayleigh scattering, but Mie scattering removed (which would incur additional variance for all techniques). Rendered at a resolution of 1024×512 on a 16-thread i7 CPU.*

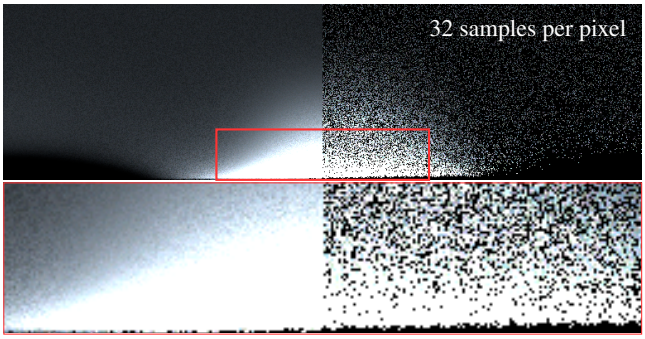

Figure 6: *Single scattering with our technique (left) compared to standard NDS [VWF18] (right), for the simple model and a Rayleigh phase function that is purposefully monochromatic, to suppress extra noise of spectral sampling. The star is 5.711° below the horizon.*

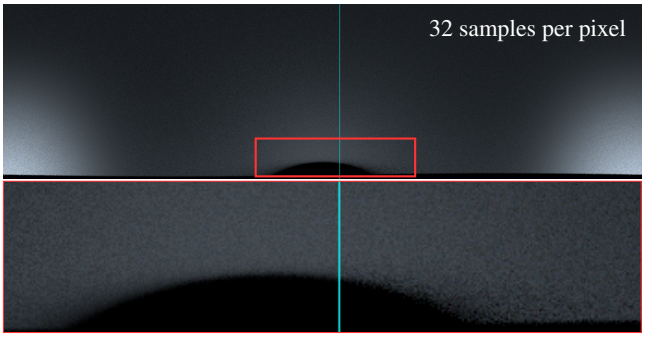

Figure 7: *Further simplification of the setting in Fig. 6 to a constant atmosphere extending to 2000 km above sea level. Our technique (left) compared to standard NDS [VWF18] (right) is less beneficial than for plausible atmospheric light transport configurations.*

4. Usage with an Approximate Analytical Atmospheric Model

We use only analytical models to build an efficient representation of an approximate earth-like atmosphere. This avoids memory accesses and incremental volume tracking schemes. Golubev [Gol20] provides detailed derivations and code that allows the transmittance to be accurately approximated analytically and inverted efficiently using Newton-Raphson iteration [BM03] for distance sampling in spherical volumes with exponential density profiles.

We model the atmosphere using such spherical exponential density profiles and using Huestis' [Hue01] approximation of the Chapman function, as proposed by Golubev [Gol20]. Our model has a scale height of 8.5 kilometers to approximate earth-like conditions.

Full Model In our full atmospheric model, the atmosphere is comprised of three layers, troposphere, stratosphere and exosphere, in order to account for varying ozone concentrations at layer boundaries of 11 km, 60 km, and 2000 km. The troposphere is modelled with an absorption of $1.32352 \times 10^{-12} m^2/mol$. The aerosols are modelled using the Cornette-Shanks phase function with $g = 0.76$ and a scattering cross-section of $1.2032 \times 10^{-12} m^2/mol$.

Simple Model Unless noted otherwise, the simple model uses only one layer with exponential falloff. Rayleigh and Liu phase functions are associated with the density. We used the Liu phase function [Liu94] as it can be sampled in closed form, while Cornette-Shanks [CS92] would require either Newton-Raphson inversion or potentially Triangle Cut Parameterization [Hei20] to sample.

5. Results and Discussion

We implemented our proposed technique in a custom spectral C++ path tracer on the CPU, using normalized distance sampling (NDS) [VWF18], hero wavelength sampling [WND*14] (without MIS), next event estimation (NEE) with solid angle sampling of the sun disk, and a volume stack [SB02] to model the atmospheric layers as analytically defined participating media. We ran our experiments on a 16-thread Intel Core i7 5960X machine, with parallel rendering of framebuffer tiles implemented in TBB. All renders are equirectangular projections to better visualize the atmosphere.

The added intersection testing and conversion of distances to the opacity domain incurs an overhead of about 17% (17 ms per sample) in a single-scattering setting.

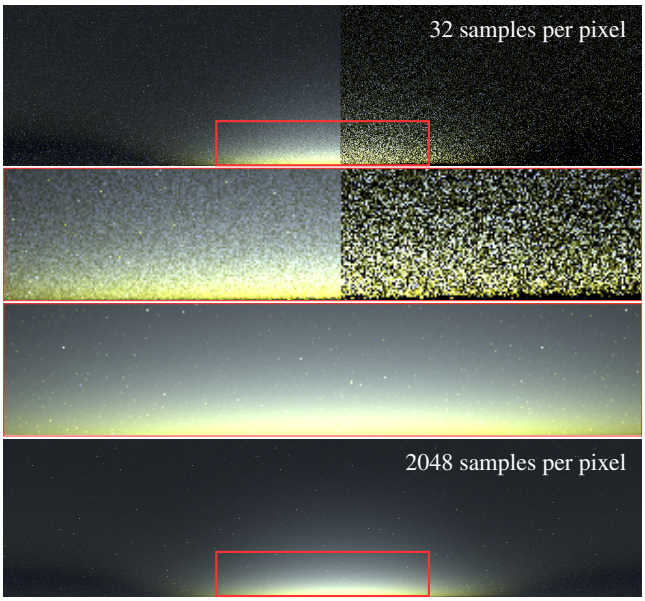

Figure 8: *Path-traced multiple scattering rendered using our technique (left) and standard NDS (right) for NEE. Shown for the more realistic, full model described in Sect. 4. The star is 5.711° below the horizon. Remaining fireflies could be handled with different MIS weighting of NEE, depending on the use case.*

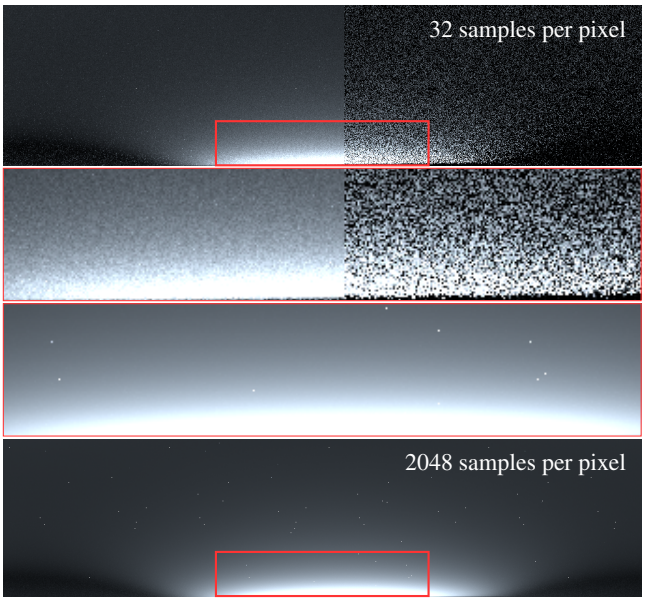

Figure 9: *Simplification of the setting in Fig. 8 to a volume with an isotropic phase function and a monochromatic cross-section. The comparison of our technique (left) to standard NDS (right) shows that transmittance variation throughout the atmosphere is a major source of variance in and of itself.*

Convergence Fig. 5 plots mean absolute error against sample count, comparing shadow-unaware sampling using only NDS to shadow-aware sampling using our proposed technique. We compare two cases of shadow-aware sampling, one where the planet is a perfect sphere and one where the occluder sphere is conservatively smaller than the lowest elevation on the planet, using a difference between highest and lowest elevation corresponding to the height of Mt. Everest. To complement this analysis, Fig. 5 also plots error over render time. Our technique improves the error in both equal-sample and equal-time comparisons. For the conservative case using a tighter shadow cylinder, the mean absolute error is approx. doubled.

Single scattering Fig. 1 compares our technique and shadow-unaware NDS in a single-scattering setting with a primitive atmospheric model of one spherical exponential density falloff for both the Rayleigh scattering and the Mie scattering (approximated by a Liu phase function). Fig. 6 further simplifies this setting, showing the Rayleigh scattering with a monochromatic cross-section, to factor out any additional noise incurred by spectral sampling. To prove the effectiveness of our technique particularly for atmospheric light transport settings, we contrast our results with exponential density profiles by also showing results for a (less realistic) constant density profile (up to 2000 kilometers above sea level) in Fig. 7. This case is noticeably less confounded by shadows in terms of convergence.

Multiple Scattering To show the effectiveness of our technique in more realistic use cases, we also provide preliminary results for multiple scattering. Fig. 8 shows the full atmospheric model (Sect. 4) and Fig. 9 shows a simplified model with isotropic scattering and monochromatic cross-section. These results are preliminary because we do not implement MIS of shadow-aware distance sampling for NEE and of emitter hits by recursive scattering via the sampling of phase functions. There are multiple ways around this issue depending on the use case, e.g. putting all MIS weight on NEE for emitter connections with participating media, or computing the shadow-aware PDF for MIS also in non-NEE path expansions.

For completeness, Fig. 10 shows a day-time setting where our technique does not bring improvements in the absence of shadowing.

6. Conclusions and Future Work

We showed the particular merits of a visibility-aware transmittance sampling technique for rendering atmospheric scattering. Our technique particularly improves NEE for single scattering. In multiple scattering, visibility on varying random walks is harder to predict and there are new sources of variance. Further investigations are required to sample these cases effectively. Guiding by e.g. Gaussian mixture models applied to the radiance of the sky [VVP21] gives a promising starting point. Building a simplified analytical sky model for the sole purpose of importance sampling could be another avenue. Due to varying indices of refraction, rays through the atmosphere are curved, especially in dusk and dawn scenes [HMS05]. Fitting a more complex shape to the curved shadow volume, future work could still leverage radial symmetry as in our case.

References

[BCRK*10] BARAN I., CHEN J., RAGAN-KELLEY J., DURAND F., LEHTINEN J.: A hierarchical volumetric shadow algorithm for single scattering. *ACM Trans. Graph. 29*, 6 (dec 2010), 178:1–178:10. doi:10.1145/1882261.1866200. 3

[BD16] BILLEN N., DUTRÉ P.: Line sampling for direct illumination. *Computer Graphics Forum 35*, 4 (2016), 45–55. doi:10.1111/cgf.12948. 3

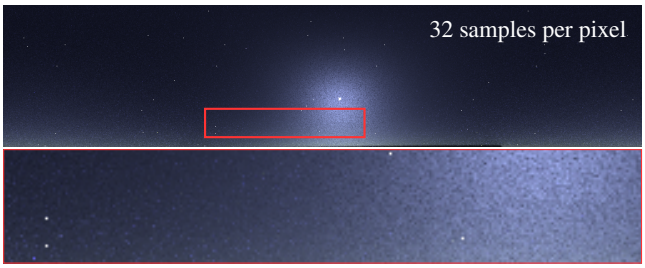

Figure 10: *A daytime scene where our technique does not improve distance sampling, shown for the full model with multiple scattering as in Fig. 8. The star is 26.565° above the horizon.*

[BJ17] BITTERLI B., JAROSZ W.: Beyond points and beams: Higher-dimensional photon samples for volumetric light transport. *ACM TOG 36*, 4 (2017), 112:1–112:12. doi:10.1145/3072959.3073698. 3

[BM03] BROWN F. B., MARTIN W. R.: Direct sampling of monte carlo flight paths in media with continuously varying cross-sections. In *Proc. ANS Mathematics & Computation Topical Meeting* (2003). 4

[Bru17] BRUNETON E.: A qualitative and quantitative evaluation of 8 clear sky models. *IEEE Trans. Vis. and Computer Graphics 23*, 12 (dec 2017), 2641–2655. doi:10.1109/tvcg.2016.2622272. 2

[BSA10] BILLETER M., SINTORN E., ASSARSSON U.: Real Time Volumetric Shadows using Polygonal Light Volumes. In *High Performance Graphics* (2010), Doggett M., Laine S., Hunt W., (Eds.), The Eurographics Association. doi:10.2312/EGGH/HPG10/039-045. 3

[CBDJ11] CHEN J., BARAN I., DURAND F., JAROSZ W.: Real-time volumetric shadows using 1d min-max mipmaps. In *Symposium on Interactive 3D Graphics and Games* (2011), I3D '11, Association for Computing Machinery, p. 39–46. doi:10.1145/1944745.1944752. 3

[Che21] CHENG H.: *Line sampling in participating media*. Master's thesis, Dartmouth College, Jun 2021. No. 40. URL: https://digitalcommons.dartmouth.edu/masters_theses/40. 3

[CS92] CORNETTE W. M., SHANKS J. G.: Physically reasonable analytic expression for the single-scattering phase function. *Appl. Opt. 31*, 16 (Jun 1992), 3152–3160. doi:10.1364/AO.31.003152. 4

[GGJ18] GUIMERA D., GUTIERREZ D., JARABO A.: A Physically-Based Spatio-Temporal Sky Model. In *Spanish Computer Graphics Conference (CEIG)* (2018), The Eurographics Association. doi:10.2312/ceig.20181150. 2

[GKH*13] GEORGIEV I., KŘIVÁNEK J., HACHISUKA T., NOWROUZEZAHRAI D., JAROSZ W.: Joint importance sampling of low-order volumetric scattering. *ACM Trans. Graph. 32*, 6 (nov 2013). doi:10.1145/2508363.2508411. 2

[Gol20] GOLUBEV E.: Sampling analytic participating media, 2020. URL: zero-radiance.github.io/post/analytic-media/. 4

[Hei20] HEITZ E.: Can't invert the cdf? the triangle-cut parameterization of the region under the curve. *Computer Graphics Forum 39*, 4 (2020), 121–132. doi:10.1111/cgf.14058. 4

[HGJ*17] HACHISUKA T., GEORGIEV I., JAROSZ W., KŘIVÁNEK J., NOWROUZEZAHRAI D.: Extended path integral formulation for volumetric transport. In *Proceedings of the Eurographics Symposium on Rendering: Experimental Ideas & Implementations* (2017), EGSR '17, EG, p. 65–70. doi:10.2312/sre.20171195. 3

[Hil20] HILLAIRE S.: A scalable and production ready sky and atmosphere rendering technique. *Computer Graphics Forum 39*, 4 (2020), 13–22. doi:10.1111/cgf.14050. 2

[HMS05] HABER J., MAGNOR M., SEIDEL H.-P.: Physically-based simulation of twilight phenomena. *ACM Trans. Graph. 24*, 4 (oct 2005), 1353–1373. doi:10.1145/1095878.1095884. 2, 5

[Hol15] HOLZSCHUCH N.: Accurate computation of single scattering in participating media with refractive boundaries. *Computer Graphics Forum 34*, 6 (2015), 48–59. doi:10.1111/cgf.12517. 2

[Hue01] HUESTIS D. L.: Accurate evaluation of the chapman function for atmospheric attenuation. *Journal of Quantitative Spectroscopy and Radiative Transfer 69*, 6 (2001), 709–721. doi:10.1016/S0022-4073(00)00107-2. 4

[HW12] HOSEK L., WILKIE A.: An analytic model for full spectral sky-dome radiance. *ACM Trans. Graph. 31*, 4 (jul 2012), 95:1–95:9. doi:10.1145/2185520.2185591. 1, 2

[Irw96] IRWIN J.: Full-spectral rendering of the earth's atmosphere using a physical model of rayleigh scattering. In *In Proc. 14th Eurographics UK Conference* (1996), pp. 103–115. 3

[KF12] KULLA C., FAJARDO M.: Importance sampling techniques for path tracing in participating media. *Comput. Graph. Forum 31*, 4 (jun 2012), 1519–1528. doi:10.1111/j.1467-8659.2012.03148.x. 2, 3

[Liu94] LIU P.: A new phase function approximating to mie scattering for radiative transport equations. *Physics in Medicine and Biology 39*, 6 (jun 1994), 1025–1036. doi:10.1088/0031-9155/39/6/008. 4

[NDN96] NISHITA T., DOBASHI Y., NAKAMAE E.: Display of clouds taking into account multiple anisotropic scattering and sky light. SIGGRAPH '96, ACM, p. 379. doi:10.1145/237170.237277. 2

[NSTN93] NISHITA T., SIRAI T., TADAMURA K., NAKAMAE E.: Display of the earth taking into account atmospheric scattering. SIGGRAPH '93, ACM, pp. 175–182. doi:10.1145/166117.166140. 2, 3

[Pho75] PHONG B. T.: Illumination for computer generated pictures. *Commun. ACM 18*, 6 (jun 1975), 311–317. doi:10.1145/360825.360839. 3

[PSM93] PEREZ R., SEALS R., MICHALSKY J.: All-weather model for sky luminance distribution—preliminary configuration and validation. *Solar Energy 50*, 3 (1993), 235–245. doi:10.1016/0038-092X(93)90017-I. 1, 2

[PSS99] PREETHAM A. J., SHIRLEY P., SMITS B.: A practical analytic model for daylight. SIGGRAPH '99, ACM Press/Addison-Wesley Publishing Co., p. 91–100. doi:10.1145/311535.311545. 1, 2

[SB02] SCHMIDT C. M., BUDGE B.: Simple nested dielectrics in ray traced images. *Journal of Graphics Tools 7*, 2 (2002), 1–8. doi:10.1080/10867651.2002.10487555. 4

[SJ19] SALESIN K., JAROSZ W.: Combining point and line samples for direct illumination. *Computer Graphics Forum 38*, 4 (2019), 159–169. doi:10.1111/cgf.13779. 3

[VM22] VELINOV Z. V., MITCHELL K.: Collimated whole volume light scattering in homogeneous finite media. *IEEE Transactions on Visualization and Computer Graphics (to appear)* (2022). doi:10.1109/TVCG.2021.3135764. 3

[VVP21] VITSAS N., VARDIS K., PAPAIOANNOU G.: Sampling Clear Sky Models using Truncated Gaussian Mixtures. In *Eurographics Symposium on Rendering - DL-only Track* (2021), Bousseau A., McGuire M., (Eds.), EG. doi:10.2312/sr.20211288. 5

[VWF18] VILLEMIN R., WRENNINGE M., FONG J.: Efficient unbiased rendering of thin participating media. *Journal of Computer Graphics Techniques (JCGT) 7*, 3 (September 2018), 50–65. URL: http://jcgt.org/published/0007/03/03/. 2, 3, 4

[WND*14] WILKIE A., NAWAZ S., DROSKE M., WEIDLICH A., HANIKA J.: Hero wavelength spectral sampling. *Computer Graphics Forum 33*, 4 (2014), 123–131. doi:10.1111/cgf.12419. 4

[WR08] WYMAN C., RAMSEY S.: Interactive volumetric shadows in participating media with single-scattering. In *IEEE Symposium on Interactive Ray Tracing* (2008), IEEE, pp. 87–92. doi:10.1109/RT.2008.4634627. 3

[WVBR*21] WILKIE A., VEVODA P., BASHFORD-ROGERS T., HOŠEK L., ISER T., KOLÁŘOVÁ M., RITTIG T., KŘIVÁNEK J.: A fitted radiance and attenuation model for realistic atmospheres. *ACM Trans. Graph. 40*, 4 (July 2021), 135:1–135:14. doi:10.1145/3450626.3459758. 2